Turning traditionally nonwetting surfaces wetting for even ultra-high surface energy liquids

Kyle L. Wilke[a,1], Zhengmao Lu[a,1], Youngsup Song[a], and Evelyn N. Wang[a,2]

[a]Department of Mechanical Engineering, Massachusetts Institute of Technology, Cambridge, MA 02139

Edited by David Weitz, Department of Physics, Division of Engineering and Applied Science, Harvard University, Cambridge, MA; received May 16, 2021; accepted December 6, 2021

We present a surface-engineering approach that turns all liquids highly wetting, including ultra-high surface tension fluids such as mercury. Previously, highly wetting behavior was only possible for intrinsically wetting liquid/material combinations through surface roughening to enable the so-called Wenzel and hemiwicking states, in which liquid fills the surface structures and causes a droplet to exhibit a low contact angle when contacting the surface. Here, we show that roughness made of reentrant structures allows for a metastable hemiwicking state even for nonwetting liquids. Our surface energy model reveals that with liquid filled in the structure, the reentrant feature creates a local energy barrier, which prevents liquid depletion from surface structures regardless of the intrinsic wettability. We experimentally demonstrated this concept with microfabricated reentrant channels. Notably, we show an apparent contact angle as low as 35° for mercury on structured silicon surfaces with fluorinated coatings, on which the intrinsic contact angle of mercury is 143°, turning a highly nonwetting liquid/material combination highly wetting through surface engineering. Our work enables highly wetting behavior for previously inaccessible material/liquid combinations and thus expands the design space for various thermofluidic applications.

hemiwicking | Cassie state | omniphobic | reentrant structures | omniphilic

Highly wetting surfaces, which are desired for a range of thermofluidic systems such as microfluidics (1, 2), antifogging (3), liquid separation (4, 5), and heat transfer enhancement via boiling and thin film evaporation (6, 7), have only been achieved for intrinsically wetting liquid/solid combinations. By roughening a substrate with an intrinsic contact angle $\theta < 90°$, the wettability will be enhanced. If the roughening is aggressive enough (*SI Appendix*, Text S1 and Fig. S1), a so-called hemiwicking state can be reached in which liquid fills the surface structures and exhibits a very low apparent contact angle θ^* (Fig. 1*A*, *i*) (8). However, for intrinsically nonwetting liquid/solid combinations ($\theta > 90°$), roughening further decreases the wettability. Aggressive roughening typically results in the repellent Cassie state instead (Fig. 1*A*, *ii*) (9). *SI Appendix*, Text S1 describes different wetting states in further detail. Because high surface tension liquids and low surface energy solids rarely render intrinsic contact angles $\theta < 45°$ (Fig. 1*B*), it is not surprising that liquids with medium-to-high surface tension such as water or mercury do not wet low surface energy materials, structured or not (10–20). Therefore, turning a nonwetting liquid/solid combination highly wetting is fundamentally significant. Moreover, it removes restrictions on material selection due to wettability requirements for thermofluidic applications. For example, fluorinated polymers have great chemical resistance due to their chemical inertness but are also generally nonwetting to water, limiting the coating's application when wetting behavior is needed. Similarly, owing to their high thermal conductivity, liquid metals are excellent working fluid candidates in high-temperature heat pipes (7, 21). However, they do not exhibit highly wetting behaviors on many solid surfaces, limiting their use (18). In this work, we turn traditionally nonwetting surfaces wetting to even high surface tension liquids using reentrant structures (Fig. 1*A*, *iii*). Such reentrant structures are excellent at creating local energy barriers to liquid propagation and have previously been used to enable liquid repellency to completely wetting fluids (i.e., the reverse behavior of what is demonstrated in this work) (*SI Appendix*, Text S2 and Fig. S2) (10, 22–28) as well as create directional steering of liquid (29). Here, we create a metastable hemiwicking state via contact line pinning on reentrant structures prefilled with nonwetting liquids and demonstrate the ability to control wetting through surface structuring and liquid manipulation alone, largely decoupling the wetting behavior from the material/liquid used as long as prefilling of the liquid is successfully achieved.

To illustrate why reentrant structures enable a metastable hemiwicking state, we model how the total surface energy varies with the liquid volume for reentrant channels initially filled with a nonwetting liquid (Fig. 2*A*). In Fig. 2*A*, *i*, the total surface energy of a unit depth of the unit cell is given by:

$$E_1^r = \gamma_{sl}(4D + l + 2H) + \gamma_{lg} l, \quad [1]$$

where γ_{sl} is the surface energy of solid–liquid interfaces, γ_{lg} is the surface energy of liquid–gas interfaces, l is the channel pitch, D is the length of the reentrant overhang, H is the channel height, and the thickness of the overhang is assumed to be minimal compared to other dimensions (Fig. 2*A*). As the liquid is gradually removed from above, more solid–liquid interfaces are replaced by solid–gas interfaces until contact line pinning occurs at the reentrant feature. Between Fig. 2*A*, *ii* and *iii*, the solid–liquid and solid–gas interface area remains the same while the liquid–gas interface area decreases, and the total surface energy can be calculated as:

Significance

Control over the interaction between liquids and surfaces is used in numerous thermofluidic systems, with behaviors ranging from highly repellent to highly wetting. In this work, we demonstrate that surface engineering enables highly wetting behavior from liquid/surface combinations that are typically nonwetting, broadening the design space for thermofluidic systems.

Author contributions: K.L.W., Z.L., and E.N.W. designed research; K.L.W., Z.L., and Y.S. performed research; K.L.W., Z.L., and Y.S. analyzed data; and K.L.W., Z.L., Y.S., and E.N.W. wrote the paper.

Competing interest statement: A patent has been filed based on this work.

This article is a PNAS Direct Submission.

[1]K.L.W. and Z.L. contributed equally to this work.

[2]To whom correspondence may be addressed. Email: enwang@mit.edu.

This article contains supporting information online at http://www.pnas.org/lookup/suppl/doi:10.1073/pnas.2109052119/-/DCSupplemental.

Published January 21, 2022.

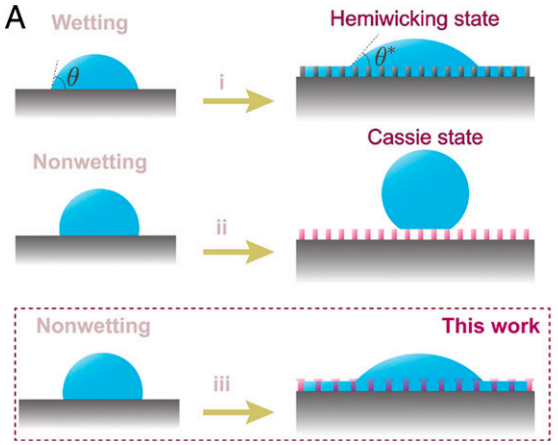

B

Typical θ (γ_s / γ_l)	Low (e.g., fluoropolymer)	Medium (e.g., nitride, oxide)	High (e.g., metal)
Low (e.g., alcohol, refrigerant)	< 90°	< 90°	< 90°
Medium (e.g., water)	> 90°	< 90°	< 90°
High (e.g., molten salt, liquid metal)	> 90°	> 90°	Mixed

Fig. 1. (*A*) Tuning contact angles for liquid/solid combinations with different intrinsic wettabilities. Surface roughening typically results in the highly wetting hemiwicking state only for intrinsically wetting liquid/solid combinations (*i*) and leads to the repellent Cassie state instead for intrinsically nonwetting combinations (*ii*). Our approach allows for a metastable hemiwicking state using surface reentrant structures, regardless of intrinsic wettabilities (*iii*). (*B*) Typical intrinsic contact angles for combinations of liquids of different surface tensions and solids with different surface energies with example references (10–20).

$$E^r_{23} = \gamma_{sl}(2D + l - d + 2H) + \gamma_{sg}(d + 2D) + 2\gamma_{lg}R_{23}\xi, \quad [2]$$

where γ_{sg} is the surface energy of solid–gas interfaces, ξ is the contact angle of the liquid front with respect to the top surface, d is the width of the channel wall, and R_{23} is the radius of curvature of the liquid–gas interface during this stage:

$$R_{23} = \frac{l - d - 2D}{2\cos\xi}. \quad [3]$$

Note that during this liquid-removal process, ξ goes from θ to zero where the interface becomes flat. Beyond $\xi = 0$, as we continue to remove the liquid, the liquid–gas interface area starts increasing and the total surface energy can be expressed as

$$E^r_{34} = \gamma_{sl}(2D + l - d + 2H) + \gamma_{sg}(d + 2D) + 2\gamma_{lg}R_{34}(\pi - \varphi), \quad [4]$$

where φ is the contact angle of the liquid front with respect to the bottom surface of the overhang, and R_{34} is the radius of curvature of the liquid–gas interface during this stage

$$R_{34} = \frac{l - d - 2D}{2\cos(\pi - \varphi)}, \quad [5]$$

where φ varies from 0 to $\pi - \theta$. This increase in surface energy from Fig. 2*A*, *iii* and *iv* creates a local energy barrier that enables a metastable hemiwicking state, avoiding a completely dry state (Fig. 2*A*, *v*). Note that to enter this metastable state, it is necessary to prefill the surface structure, which is different from a typical hemiwicking state. On the other hand, for normal channels (no reentrant structure) initially filled with a nonwetting liquid (Fig. 2*B*, *i*), pinning still occurs as we remove liquid from the top (Fig. 2*B*, *ii*). However, once the contact angle with respect to the side wall reaches θ (Fig. 2*B*, *iii*), the interface further recedes, leading to the complete dry state (Fig. 2*B*, *iv*). Accordingly, the total surface energy decreases monotonically during the liquid-removal process from normal channels, and no metastable hemiwicking state is observed. The detailed surface energy calculation for nonreentrant channels can be found in *SI Appendix*, Text S3. In Fig. 2 *A* and *B*, we also plot the total surface energy as a function of the liquid volume for reentrant and nonreentrant structures, respectively, setting $\theta = 135°$ and normalizing the total surface energy and the liquid volume to take values between 0 and 1. While the values in Fig. 2 *A* and *B* do not have specific physical meanings, the trend shows that a metastable energy state (a local energy minimum) only exists for reentrant structures.

The result in Fig. 2*B*, showing that the normal channels (nonreentrant channels) cannot maintain a filled state for nonwetting liquids is consistent with literature. Previously, researches have shown which wetting states are stable for liquids of different contact angles on structured surfaces. For nonwetting liquids, the Wenzel and hemiwicking states are

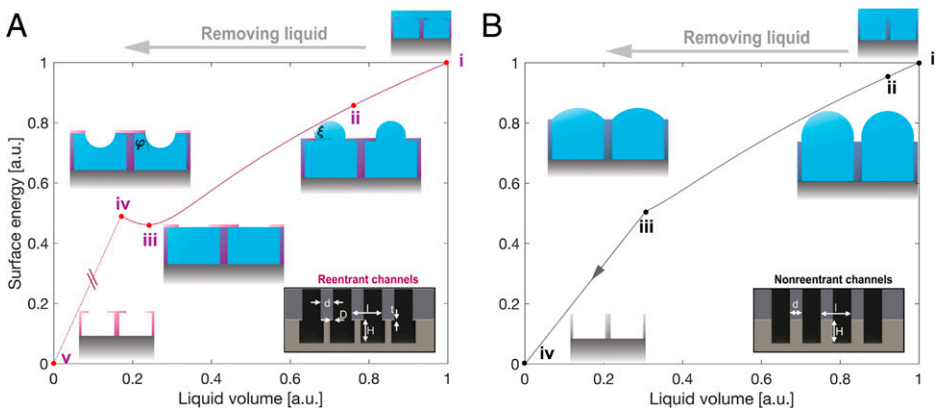

Fig. 2. Reentrant structures enabling a highly wetting state. (*A*) A reentrant structure initially filled with a nonwetting liquid begins emptying (*i*). The three-phase contact line pins at the reentrant feature (*ii* through *iv*), creating a local energy barrier to prevent complete dry out (*v*). (*B*) A nonreentrant structure initially filled with a nonwetting liquid begins emptying (*i*). Pinning still occurs (*ii* and *iii*), but the interface recedes on the side wall before it becomes flat, which fails to create any local energy barrier, leading to the complete dry state (*iv*).

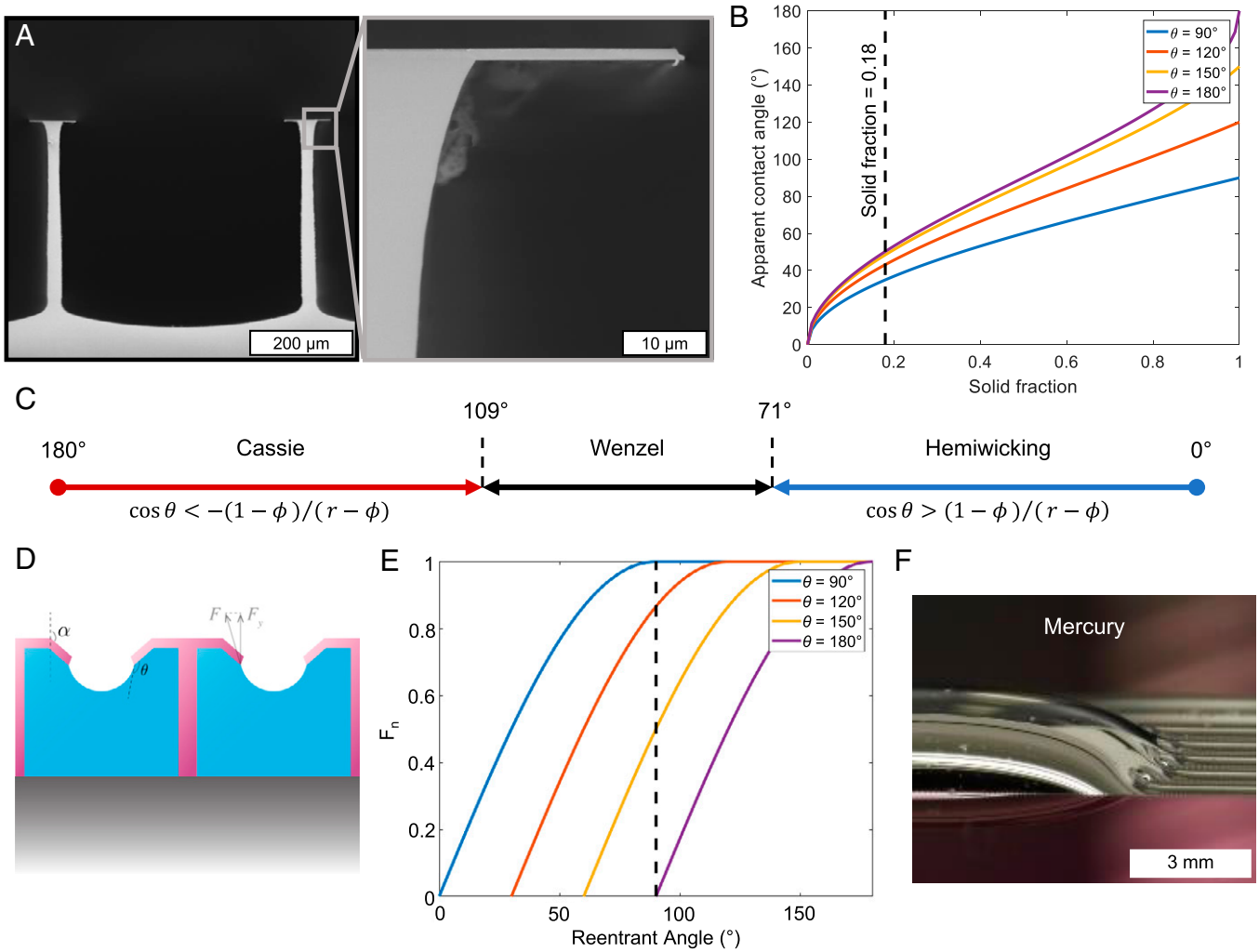

Fig. 3. Fabricated reentrant surfaces. (*A*) Cross-section scanning electron microscope images of a cleaved section of a reentrant channel surface used in this work. Surfaces had up to 10 channels to allow for sufficient area to characterize the apparent contact angle on the surface. (*B*) Expected apparent contact angle for surfaces with varied projected solid fraction based on the hemiwicking equation (*SI Appendix*, Eq. **S2**). A projected solid fraction of 0.18 was chosen in this work, as it will achieve wetting behavior for liquids with highly nonwetting intrinsic contact angles (i.e., approaching 180°). (*C*) Schematic depicting when the Cassie, Wenzel, and hemiwicking states would typically be expected for the surfaces used in this work. (*D*) A nonwetting liquid confined within reentrant channels, with a reentrant angle, α, has a component of its total surface tension force, F, that acts in the vertical direction, F_y, which acts to hold the liquid in the channel despite its nonwetting contact angle. (*E*) Normalized surface tension force, F_n, that creates the metastable hemiwicking state. (*F*) Image of the three-phase contact line for mercury on top of a prefilled reentrant channel surface. Because the liquid interacts with a hemiwicking surface consisting of nonwetting channel wall tops and wetting liquid within the channels, the three-phase contact line forms a complex shape. Above the nonwetting channel walls, the liquid is pushed back into the drop, while the wetting liquid within the channel pulls the liquid forward away from the drop, creating a fingered appearance of the contact line. This complex three-phase contact line also shows that the liquid within the reentrant channels is completely confined to the channel even when additional liquid like the droplets seen in these photos is added on top of the channels.

often not stable. One can predict the critical intrinsic contact angle that separates when each of the three wetting states, Cassie, Wenzel, or hemiwicking is energetically favorable. When $\cos\theta > (1-\phi)/(r-\phi)$, the hemiwicking state is most energetically favorable, where θ is the intrinsic contact angle on the surface, ϕ is the projected solid fraction (also called the area fraction), and r is the surface roughness. Meanwhile, when $\cos\theta < -(1-\phi)/(r-\phi)$, the Cassie state is favorable, and at intermediate contact angles, the Wenzel state is most favorable (8, 30, 31). By observation, we see that typically, the hemiwicking state is only favorable for wetting liquids.

Fabricated Reentrant Microstructures

To experimentally demonstrate that reentrant structures enable wetting of ultra-high surface tension fluids, we fabricated reentrant microchannels (Fig. 3*A*) as well as normal microchannels. Channels were chosen due to the simplicity of fabrication and the well-established understanding of typical wetting behavior (32). The full fabrication process is described in *SI Appendix*, Fig. S3 and *Materials and Methods*. We fabricated reentrant channels with l = 500 μm, H = 400 μm, d = 40 μm, t = 1 μm, and D = 25 μm and normal channels with l = 500 μm, H = 400 μm, and d = 90 μm. *SI Appendix*, Table S1 summarizes the geometry of tested samples. All surfaces were also coated with a conformal, 60-nm-thick low surface energy polymer (C_4F_8). In fact, because the coating is a low surface energy material, it generally renders the surface more repellent, making a demonstration of wetting of ultra-high surface tension liquids even more difficult. Nevertheless, by using the reentrant channels with a projected solid fraction of $\phi = (d+2D)/l = 0.18$, we can obtain a surface with an apparent contact angle less than 50° for even highly nonwetting liquids (Fig. 3*B*) based on the

equation for apparent contact angle in the hemiwicking wetting state (*SI Appendix*, Eq. **S2**). For the normal channels in this work, $\phi = d/l = 0.18$ and $r = 2.6$, while r for the reentrant channels was 2.7. Therefore, liquids with contact angles above ~109° are not stable in the Wenzel state (i.e., they transition automatically to the Cassie state), and liquids with contact angles below ~71° exhibit the hemiwicking state, and those in between are most stable in the Wenzel state (Fig. 3*C*). For the surfaces used in this work, mercury and water had an advancing and receding contact angle higher than where the Wenzel state can be stable, and all the nonwetting liquids used would not have a stable hemiwicking state.

Next, to determine what level of reentrance was required, we adopted the framework used by K.L.W. for omniphobic surfaces (33), in which a normalized surface tension force, F_n, is calculated as the ratio of the total surface tension force, F, divided by the component that holds the liquid within the channels, F_y (Fig. 3*D*). In Fig. 3*E*, the normalized surface tension force is plotted for liquids with different intrinsic contact angle, as the reentrant angle, α, is varied between 0° (normal channels) and 180° (doubly reentrant channels such as those in fabricated by Liu et al.) (10). If this force is 0 or below, no local energy minimum exists to maintain the hemiwicking state. When $F_n = 1$, the given geometry can generate the maximum energy barrier possible by changing the reentrant angle alone. From Fig. 3*E*, we see that when the reentrant angle is 0° (normal channels), F_n is equal or less than 0 for all nonwetting liquids, thus the inability of normal channels to retain nonwetting liquids. However, as the reentrant angle is increased, F_n also increases. At a reentrant angle of 90° (vertical dashed line), even liquids with a contact angle as high as 150° exhibit $F_n = 0.5$ (i.e., half of its maximum possible value). Structures with a reentrant angle above 90° are referred to as doubly reentrant structures and are difficult to manufacture (10). Therefore, a reentrant angle of 90° was used, given it is straightforward to produce, and it is sufficient for even very nonwetting liquids like mercury with a contact angle just shy of 150°. Therefore, after prefilling with mercury, liquid mercury is trapped in the reentrant channels, and a mercury droplet on top of the channel exhibits the hemiwicking state with a wetting contact angle (Fig. 3*F*). This trapped mercury is also stable to liquid flowing over the channel and then departing from the surface (Movie S1).

Apparent Wettability Independent of Intrinsic Wettability

We measured the apparent contact angle (θ^*) for a variety of liquids with different intrinsic contact angles (θ) ranging from highly wetting to highly nonwetting (liquid properties listed in *SI Appendix*, Table S2). A syringe was used to add and remove a droplet from the surface, while a camera recorded the apparent contact angle, as the droplet's three-phase contact line advanced and receded along to the channels (refer to *SI Appendix*, Text S4 and Fig. S4 for more information on wetting on channels). This technique is well-established and commonly used to quickly and accurately capture wetting behavior on surfaces (34). Therefore, despite the presence of the syringe, which wasn't depicted in schematics in Figs. 1 and 2, the measurement still captures expected behavior. When liquid contacts a microstructured surface, three distinct wetting states occur. First is the wicking state, which typically only occurs for highly wetting liquids, called the hemiwicking state (35). In this state, liquid completely fills the microstructure (*SI Appendix*, Fig. S1*A*). Second is an intermediate state that occurs for moderately wetting liquids, called the Wenzel state (36). In the Wenzel state, liquid only fills the structure below the droplet (*SI Appendix*, Fig. S1*B*). Third is the repellent state which typically only occurs for nonwetting liquids, called the Cassie state (9). In the Cassie state, air is trapped in the structures below the droplet (*SI Appendix*, Fig. S1*C*). Further discussion on these wetting states, their governing equations, and when they occur may be found in *SI Appendix*, Text S1.

In Fig. 4*A*, we show the measured apparent contact angle (θ^*) for normal channels (not prefilled) and prefilled reentrant channels. The normal channels highlighted typical wetting behavior (red symbols in Fig. 4*A*), in which highly wetting liquids ($\theta < 90°$) formed the hemiwicking state (Movie S2), moderately wetting liquids formed the Wenzel state (Movie S3), and nonwetting liquids ($\theta > 90°$) formed the Cassie state (Movie S4), consistent with previous literature (8, 37). Squares denote the advancing contact angle, while triangles denote the receding contact angle. Note that the Cassie state was observed at contact angles less than the critical angle due to a commonly observed metastable Cassie state (38). However, we also show that by first filling the reentrant channels with the same liquid as that in the syringe (i.e., placing the surface into a metastable hemiwicking state), highly wetting behavior was also extended to nonwetting liquids (blue symbols and Movie S5). As such, *SI Appendix*, Eq. **S2** for the hemiwicking state governed the wetting behavior, and a small apparent contact angle was achieved for all liquids regardless of intrinsic contact angle. We note that because the surface requires prefilling, this is different from the traditional hemiwicking state in which liquid spontaneously fills the surface. Two straightforward prefilling strategies were used in this work, demonstrating flexibility in achieving the metastable hemiwicking state (*Prefilling Surface Structures*). Using this approach, a combination of reentrant structures and prefilling, a typically highly nonwetting liquid such as mercury exhibited highly wetting behaviors. On a flat, unstructured surface, the mercury was highly nonwetting with a contact angle of 143° (Fig. 4 *B*, *i* and Movie S6). As such, on normal channels, the mercury formed the Cassie state with a contact angle of 153° (Fig. 4 *B*, *ii* and Movie S7). In comparison, the contact angle on the reentrant surface was less than 35°, highlighting this approach's ability to use surface-engineering to produce highly wetting behavior for highly nonwetting liquid/surface combinations (Fig. 4 *B*, *iii*; refer to Movie S8 for the advancing droplet and Movie S9 for the receding droplet). Even with prefilling, normal channels could not exhibit this behavior due to the energy analysis in Figs. 2*B* and 3*C*, which was also confirmed theoretically and experimentally (*SI Appendix*, Text S5).

Discussion of Limitations and Other Designs

While the wetting behavior of nonwetting liquid/solid combinations reported here is distinct from traditional hemiwicking in that it requires prefilling, it does allow nonwetting liquid contacting the surface to be wicked through the prefilled channels, as seen in Movie S5, in which a nonwetting droplet of water is pulled into the reentrant channels after initially contacting a flat, unstructured, and nonwetting portion of the surface. In other words, after placing the surface into the hemiwicking state, more traditional wicking behavior was observed. This can be used to not only enable wicking of liquids that could previously not be wicked but could also enhance the wicking performance or relax surface design constraints when wicking moderately wetting liquids.

We also show that the ability for the surface to wick addresses a potential failure mechanism of the surface, depletion of the liquid in the reentrant channels due to evaporation, which has been observed in similar systems that rely on filled surface structures to achieve a wetting behavior, such as lubricant impregnated surfaces (LIS). Despite this practical challenge, LIS has found many potential beneficial applications. For LIS, it has been shown that liquid depletion can easily be overcome by periodically refilling the impregnated liquid (39). Inspired by this approach, we demonstrate the feasibility of

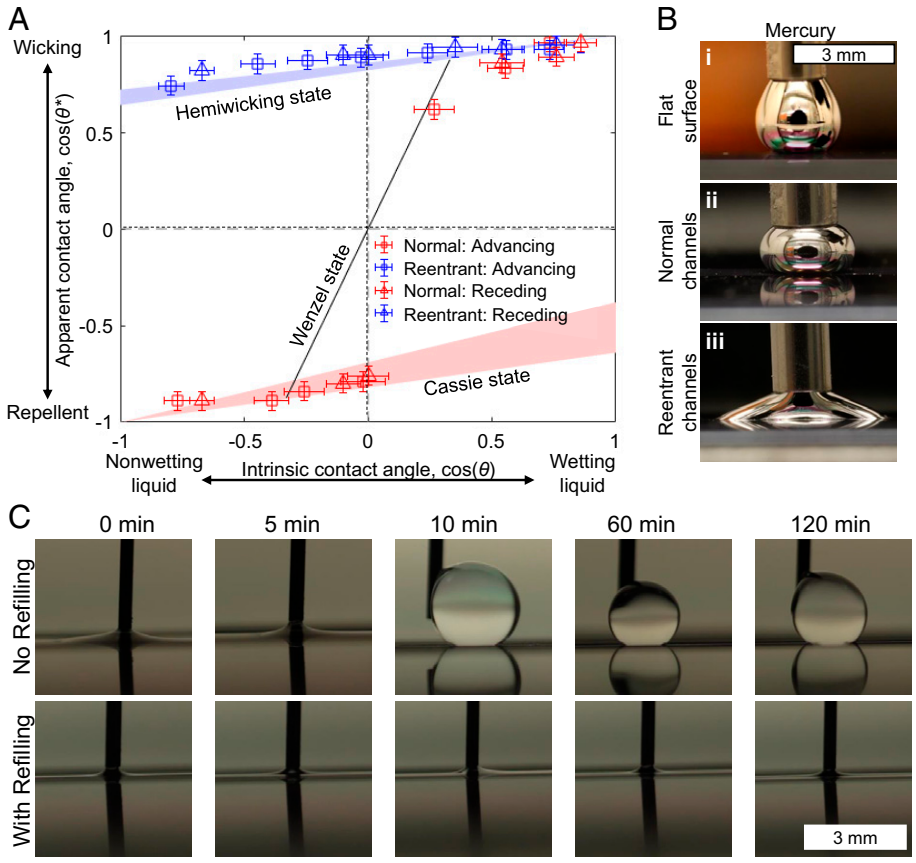

Fig. 4. Wetting even highly nonwetting liquids. (*A*) Cosine of apparent advancing contact angle (θ^*) on normal (not prefilled) and prefilled reentrant microstructures as the droplet grows along the channels for liquids with different intrinsic wettability (cos θ). The normal channels (not prefilled) highlight typical behavior, in which nonwetting liquids form a Cassie wetting state with large apparent contact angle, while wetting liquids form a hemiwicking state with small apparent contact angle. Prefilled reentrant channels, however, enable the hemiwicking state to be extended to even ultra-high surface tension liquids. The bands of expected contact angles for the hemiwicking and Cassie state are shown due to a grating error in our measurement (i.e., a droplet may orient itself on the surface in a way that the solid fraction at the contact line deviates from 0.18). This error is described in more detail in *SI Appendix*, Text S6. Contact angle measurements may be found in *SI Appendix*, Table S3. (*B*) Images of a nonwetting liquid (mercury) on a flat surface, normal channels, and reentrant channels. Because the reentrant channels are in the metastable hemiwicking state, wetting behavior is observed even for the highly nonwetting liquid mercury. (*C*) Contact angle of water on prefilled reentrant channel surfaces over time with and without periodic refilling of the water within the channel. Refilling prevents liquid depletion and prevents a transition out of the hemiwicking state.

refilling these surfaces to increase longevity of the hemiwicking state by leveraging the prefilled reentrant surface's ability to wick nonwetting liquids. We conducted experiments in which one water-prefilled, C_4F_8-coated reentrant surface did not get replenished with liquid, while a second was replenished periodically by adding a droplet to the surface, which wicked into and refilled the prefilled reentrant channels in the hemiwicking state (similar to Movie S5). We then compared how long the surface could remain in the highly wetting hemiwicking state for the surfaces with and without liquid replenishment, the result of which is shown in Fig. 4*C*. Note that in Fig. 4*C*, every data point in the without refilling sequence requires a separate experiment given that adding a droplet of liquid for contact angle measurements also replenishes liquid in the channels. The separate experiments caused slight variation in the images throughout the sequence. Due to evaporation of the water within the channels, the surface without refilling lost its hemiwicking state within 10 min, instead reverting to a Cassie state as the water in the channel was replaced with air. On the other hand, the surface with refilling remained in the hemiwicking state for 120 min before stopping the experiment, demonstrating the ability to maintain the highly wetting state with simple refilling strategies. In this case, refilling was conducted every 5 min based on the results of the surface without refilling. In these images, because the surface quickly wicks liquid in while the droplet is still small, the contact angle in the images appears less than the case in which a larger droplet was maintained on the surface. Continuing to draw analogies with LIS, depletion is also not a concern for liquids with low volatility. For instance, the first sample that we infused with mercury for this project (in August 2018) remained filled with mercury until the submission of this manuscript. Finally, for closed systems, liquid depletion in the surface structure will also usually not occur because of the saturated environment, which limits evaporation.

In this work, we also only demonstrated turning surfaces wetting to nonwetting liquids using channels. However, other geometry should be able to maintain the metastable hemiwicking state. We have added simulation demonstrating each geometry can exhibit a local energy minimum for the hemiwicking state. We performed the same modeling of the surface energy as a function of liquid volume in different reentrant structures including reentrant cavities and reentrant pillars, which showed that these geometries can produce the same local energy

minimum that maintains nonwetting liquid in the hemiwicking state (*SI Appendix*, Text S7). By then using previously modified Cassie–Baxter equations for liquid wetting on structured surfaces (32), we also predict the expected advancing and receding contact angles on these surfaces in *SI Appendix*, Text S7, which suggests that wetting behavior of nonwetting liquids can be greatly enhanced for both pillars and cavities; however, cavities are expected to have large contact angle hysteresis. The chosen geometry will also not only influence the apparent contact angle on the surface but also the stability of the metastable state and the ability to properly fill the surface, also discussed in *SI Appendix*, Text S7. Again drawing analogies to previous works designing omniphobic surfaces, which explored the effect of design parameters such as geometry and wettability on the stability of metastable wetting states (40, 41), we expect the stability of the metastable state to be improved by increasing the reentrant angle and decreasing pitch; however, decreasing the pitch could prevent vacuum-filling given the breakthrough pressure to force nonwetting liquid into the structures would be increased (*SI Appendix*, Text S7). On the other hand, design aspects such as making the ratio of the channel depth to the pitch too small could reduce the stability of the metastable hemiwicking state (39).

Finally, we only demonstrated turning surfaces wetting to nonwetting liquids using channels filled with the same liquid. However, it is likely that there are combinations of liquids filled in the channels and liquids contacting the surface that also enable this phenomenon (i.e., a different liquid in the channel as contacting the surface). We demonstrated a simple case, in which two different miscible liquids were used to show experimentally that using the same liquid is not a requirement to achieve hemiwicking. In Movie S10, we prefilled a reentrant channel surface with ethanol and then used a syringe to add water to the surface. Because the two liquids are miscible, the water was wicked away just as it would have been had it been contacting a reentrant channel surface prefilled with water. Next, in Movie S11, we did the opposite, in which we prefilled the reentrant surface with water and then used the syringe to add ethanol. Once again, the surface wicked the ethanol away. In the case on nonmiscible liquids, the behavior is expected to be more complicated and is expected to be similar to wetting behavior on LIS. However, because the reentrant surfaces create metastable states that extend wetting behavior, the use of reentrant structures for LIS is expected to increase stability of LIS wetting states and increase the potential combinations of liquids that can be used. For example, a typical design criterion for LIS is that "the lubricating liquid must wick into, wet and stably adhere within the substrate," which would have previously been limited to only wetting liquids due to the assumption that wetting is required to create a stable liquid layer on a surface (42).

Conclusion

We have demonstrated that highly wetting behavior can be achieved with surface reentrant structures, regardless of intrinsic wettabilities, by creating a metastable hemiwicking state. This metastable state enables rational control over wetting behavior independent of surface energies of the material/liquid used. Our model suggests that the local energy barrier created by the reentrant features allows for a metastable state in which liquid is maintained inside the surface structures even though it is intrinsically nonwetting. Experimentally, we showed that even ultra-high surface tension liquids such as mercury can exhibit wetting apparent contact angles with this surface design. Although challenges remain in fabrication of reentrant surfaces, this concept promises to impact technologies that utilize tailored wettability.

Materials and Methods

Fabrication of Surfaces. The fabrication procedure of both normal and reentrant channels is depicted in *SI Appendix*, Fig. S3. Each step is described in further detail here.

Photoresist exposure and development. A 2.5-μm layer of photoresist (Microposit S1822) was spin coated on polished silicon wafers that had a 1-μm-thick silicon dioxide layer on the surface. The photoresist was exposed using an MLA150 Maskless Aligner. The resist was developed for 120 s in Microposit MF CD26 developer (*SI Appendix*, Fig. S3, i).

Reactive ion etch. The silicon dioxide was first etched using CF_4 (Multiplex reactive ion etcher [MPX/LPX RIE], STS). Then, the channels were etched in the silicon with deep reactive ion etching (Rapier deep reactive ion etcher [Rapier DRIE], SPTS) (*SI Appendix*, Fig. S3, ii).

Oxide removal. For normal channels, the silicon dioxide was removed by placing the samples in 7:1 buffered oxide etch solution for 10 min (*SI Appendix*, Fig. S3*A*, iii).

SF_6 etch. An isotropic SF_6 etch (Rapier DRIE, SPTS) was used to remove silicon below the silicon dioxide to create the reentrant geometry (*SI Appendix*, Fig. S3*B*, iii).

C_4F_8 deposition. A conformal, 60-nm-thick hydrophobic polymer (C_4F_8) was deposited (Rapier DRIE, SPTS). This allowed a large range of intrinsic contact angles to be tested and created surfaces with uniform and consistent wettability (*SI Appendix*, Fig. S3, iv).

Contact Angle Measurements. A custom-built experimental setup was used to measure contact angle (*SI Appendix*, Fig. S5). The air and liquid temperature remained close to the surrounding laboratory temperature. A syringe pump (Micro4, World Precision Instruments) was used to add and remove water from a droplet on the surface. Note that the liquid was added and removed slowly enough that there was no dynamic effect on the contact angle (i.e., the capillary number was small). A digital single-lens reflex camera (EOS Rebel T3, Cannon) and macro lens were used to collect images of the droplet advancing on the surface. Lighting of the droplet was supplied with a light source (Intenselight C-HGFI, Nikon) and lens (C-HGFIB, Nikon). Contact angle was extracted from the images using ImageJ. For contact angle measurements of reentrant surfaces in the repellent state, the droplet was added to a dry surface (i.e., air within the surface structures). For the hemiwicking state, the droplet was added to a surface prefilled with the same liquid as that in the syringe. This contact angle measurement is well established, and the presence of the syringe does not create enough error to change conclusions in this work (34).

Prefilling Surface Structures. Prefilling the reentrant channels with liquid was achieved using a variety of methods. For naturally wicking liquids, the liquid was added to one end of the channels and, in turn, filled the channels spontaneously. For ethanol/water mixtures that were not wicking, the channels were first filled with pure ethanol. Next, the ethanol filled sample was placed in a large container of the ethanol/water mixture to be tested. The pure ethanol within the surface structures diffused into the mixture, thereby replacing the ethanol in the channels with the mixture. Note that the volume of ethanol in the channels was on the order of 10 μL, whereas the container was more than 1,000 times this size. Therefore, this filling method did not affect the final concentration of the mixture. Samples were then removed from the mixture such that the channels remained filled to conduct contact angle or capillary height measurements. For mercury, prefilling was achieved by vacuum-filling the reentrant microstructures. The surface was placed in a small chamber, and the chamber was then evacuated of air to less than 10 kPa, after which the chamber was filled with mercury, thereby ensuring the reentrant structures were filled with this highly nonwetting liquid. We note that the effectiveness of vacuum prefilling will be influenced by the feature size. In general, smaller surface features will require higher pressures to properly fill the structures, as described in *SI Appendix*, Text S7 and Eqs. **S9**–**S11**. Therefore, for smaller features, vacuum alone may not be enough to prefill a surface, and additional pressure may need to be applied, a trade-off that needs to be considered when applying our approach to turn a nonwetting surface wetting. The normal channels were not prefilled for experiments unless otherwise stated.

Data Availability. All study data are included in the article and/or supporting information.

ACKNOWLEDGMENTS. This work was performed in part at the Center for Nanoscale Systems (CNS), a member of the National Nanotechnology Infrastructure Network, which is supported by the NSF under NSF award no.

1541959. CNS is part of Harvard University. We gratefully acknowledge the technical support from the NanoStructures Laboratory and Microsystems Technology Laboratories at Massachusetts Institute of Technology (MIT). This work was supported by the Cooperative Agreement between the Masdar Institute of Science and Technology, Abu Dhabi, United Arab Emirates, and the MIT, Cambridge, MA—Reference no. 02/MI/MIT/CP/11/07633/GEN/G/00. Z.L. acknowledges funding support from the Air Force Office of Scientific Research with Dr. Ali Sayir as program manager.

1. P. Comanns *et al.*, Directional, passive liquid transport: The Texas horned lizard as a model for a biomimetic 'liquid diode'. *J. R. Soc. Interface* **12**, 20150415 (2015).
2. C. K. Camplisson, K. M. Schilling, W. L. Pedrotti, H. A. Stone, A. W. Martinez, Two-ply channels for faster wicking in paper-based microfluidic devices. *Lab Chip* **15**, 4461–4466 (2015).
3. R. Wang *et al.*, Light-induced amphiphilic surfaces. *Nature* **388**, 431 (1997).
4. J. Yang *et al.*, Superhydrophilic–superoleophobic coatings. *J. Mater. Chem.* **22**, 2834–2837 (2012).
5. L. Feng *et al.*, A super-hydrophobic and super-oleophilic coating mesh film for the separation of oil and water. *Angew. Chem. Int. Ed. Engl.* **116**, 2046–2048 (2004).
6. Y. Zhu *et al.*, Prediction and characterization of dry-out heat flux in micropillar wick structures. *Langmuir* **32**, 1920–1927 (2016).
7. A. Faghri, *Heat Pipe Science and Technology* (Global Digital Press, 1995).
8. D. Quéré, Wetting and roughness. *Annu. Rev. Mater. Res.* **38**, 71–99 (2008).
9. A. Cassie, S. Baxter, Wettability of porous surfaces. *Trans. Faraday Soc.* **40**, 546–551 (1944).
10. T. L. Liu, C.-J. Kim, Repellent surfaces. Turning a surface superrepellent even to completely wetting liquids. *Science* **346**, 1096–1100 (2014).
11. S. Lee, J.-S. Park, T. R. Lee, The wettability of fluoropolymer surfaces: Influence of surface dipoles. *Langmuir* **24**, 4817–4826 (2008).
12. S. Spencer, G. Andrews, C. Deacon, Contact angle of ethanol–water solutions on crystalline and mesoporous silicon. *Semicond. Sci. Technol.* **28**, 055011 (2013).
13. X. Lu, J. Liu, X. Xu, Contact angle measurements of pure refrigerants. *Int. J. Heat Mass Transf.* **102**, 877–883 (2016).
14. L. T. Fan *et al.*, Contact angle of ethanol and n-propanol aqueous solutions on metal surfaces. *Chem. Eng. Technol.* **34**, 1535–1542 (2011).
15. T. Yasuda, T. Okuno, H. Yasuda, Contact angle of water on polymer surfaces. *Langmuir* **10**, 2435–2439 (1994).
16. K. Bewig, W. Zisman, The wetting of gold and platinum by water. *J. Phys. Chem.* **69**, 4238–4242 (1965).
17. T. Smith, The hydrophilic nature of a clean gold surface. *J. Colloid Interface Sci.* **75**, 51–55 (1980).
18. A. H. Ellison, R. Klemm, A. M. Schwartz, L. Grubb, D. A. Petrash, Contact angles of mercury on various surfaces and the effect of temperature. *J. Chem. Eng. Data* **12**, 607–609 (1967).
19. A. Bondi, The spreading of liquid metals on solid surfaces. Surface chemistry of high-energy substances. *Chem. Rev.* **52**, 417–458 (1953).
20. I. D. Joshipura *et al.*, Patterning and reversible actuation of liquid gallium alloys by preventing adhesion on rough surfaces. *ACS Appl. Mater. Interfaces* **10**, 44686–44695 (2018).
21. D. Reay, R. McGlen, P. Kew, *Heat Pipes: Theory, Design and Applications* (Butterworth-Heinemann, 2013).
22. E. S. Savoy, F. A. Escobedo, Simulation study of free-energy barriers in the wetting transition of an oily fluid on a rough surface with reentrant geometry. *Langmuir* **28**, 16080–16090 (2012).
23. E. M. Domingues, S. Arunachalam, H. Mishra, Doubly reentrant cavities prevent catastrophic wetting transitions on intrinsically wetting surfaces. *ACS Appl. Mater. Interfaces* **9**, 21532–21538 (2017).
24. E. M. Domingues, S. Arunachalam, J. Nauruzbayeva, H. Mishra, Biomimetic coating-free surfaces for long-term entrapment of air under wetting liquids. *Nat. Commun.* **9**, 3606 (2018).
25. J. R. Panter, Y. Gizaw, H. Kusumaatmaja, Multifaceted design optimization for superomniphobic surfaces. *Sci. Adv.* **5**, eaav7328 (2019).
26. G.-T. Yun *et al.*, Springtail-inspired superomniphobic surface with extreme pressure resistance. *Sci. Adv.* **4**, eaat4978 (2018).
27. J. Li *et al.*, Topological liquid diode. *Sci. Adv.* **3**, eaao3530 (2017).
28. K. L. Wilke, D. J. Preston, Z. Lu, E. N. Wang, Toward condensation-resistant omniphobic surfaces. *ACS Nano* **12**, 11013–11021 (2018).
29. S. Feng *et al.*, Three-dimensional capillary ratchet-induced liquid directional steering. *Science* **373**, 1344–1348 (2021).
30. P.-G. De Gennes, Wetting: Statics and dynamics. *Rev. Mod. Phys.* **57**, 827 (1985).
31. P.-G. De Gennes, F. Brochard-Wyart, D. Quéré, *Capillarity and Wetting Phenomena: Drops, Bubbles, Pearls, Waves* (Springer Science & Business Media, 2013).
32. W. Choi, A. Tuteja, J. M. Mabry, R. E. Cohen, G. H. McKinley, A modified Cassie-Baxter relationship to explain contact angle hysteresis and anisotropy on non-wetting textured surfaces. *J. Colloid Interface Sci.* **339**, 208–216 (2009).
33 K. L. Wilke, M. Garcia, D. J.. Preston, E. N. Wang, "A simple fabrication method for doubly reentrant omniphobic surfaces via stress induced bending in *Hilton Head Workshop 2018: A Solid-State Sensors, Actuators and Microsystems Workshop* (2018). 10.31438/trf.hh2018.74. Accessed 13 January 2022.
34. T. Huhtamäki, X. Tian, J. T. Korhonen, R. H. A. Ras, Surface-wetting characterization using contact-angle measurements. *Nat. Protoc.* **13**, 1521–1538 (2018).
35. R. Dettre, R. Johnson, Contact angle hysteresis, I. Study of an idealized rough surface. *Adv. Chem. Ser.* **43**, 112 (1964).
36. R. N. Wenzel, Resistance of solid surfaces to wetting by water. *Ind. Eng. Chem.* **28**, 988–994 (1936).
37. S. Shibuichi, T. Onda, N. Satoh, K. Tsujii, Super water-repellent surfaces resulting from fractal structure. *J. Phys. Chem.* **100**, 19512–19517 (1996).
38. A. Lafuma, D. Quéré, Superhydrophobic states. *Nat. Mater.* **2**, 457–460 (2003).
39. D. Seo, J. Shim, C. Lee, Y. Nam, Brushed lubricant-impregnated surfaces (BLIS) for long-lasting high condensation heat transfer. *Sci. Rep.* **10**, 2959 (2020).
40. A. Tuteja, W. Choi, J. M. Mabry, G. H. McKinley, R. E. Cohen, Robust omniphobic surfaces. *Proc. Natl. Acad. Sci. U.S.A.* **105**, 18200–18205 (2008).
41. A. Tuteja *et al.*, Designing superoleophobic surfaces. *Science* **318**, 1618–1622 (2007).
42. T.-S. Wong *et al.*, Bioinspired self-repairing slippery surfaces with pressure-stable omniphobicity. *Nature* **477**, 443–447 (2011).